

**ESTIMATION OF THE VOLUME OF THREE-DIMENSIONAL SUBSURFACE  
VOIDS USING THREE-DIPOLE RADAR**

(Translation from Proceedings of JSCE, No.592/V-39, May 1998)



Seok-Kyun PARK



Taketo UOMOTO

The presence of voids under pavements or behind tunnel linings results in their deterioration. One proposed method of effectively detecting such voids by non-destructive means is radar. This research is devoted to quantitatively evaluating the efficiency of such non-destructive tests with radar. As a foundation to this ongoing research, which aims to acquire directional information and estimate the volume of three-dimensional voids using three-dipole radar, an investigation of microwave polarization methods is carried out with various void orientations and void geometries. As a result, it is clarified that the response of microwave polarization modes depends on void geometry and thus there is a possibility of identifying the geometry and orientation of specific voids by the microwave polarization method. Further, with the addition of a method for acquiring the thickness of voids, the availability of this method for estimating the volume of three-dimensional voids is investigated.

*Keywords : radar, void, volume, microwave polarization, concrete*

---

Seok-Kyun Park is an Assistant Professor in the Department of Civil Engineering at Taejon University, Taejon, Korea. He obtained his D.Eng. from Tokyo University in 1995. His research interests relate to image processing and simulation of radar response to subsurface objects in concrete. He is a member of the JSCE.

---

Taketo Uomoto is a Professor at the Institute of Industrial Science at Tokyo University, Tokyo, Japan. He obtained his D.Eng. from Tokyo University in 1981. His research interests relate to nondestructive testing, the shape optimization of structures, the durability of concrete, new composite materials, the computer simulation of cement hydration, the evaluation of concrete structure deterioration, and analytical computer modeling phenomena, as well as the durability of shotcrete and self-compacting concrete. He is a fellow of the JSCE.

---

## 1. INTRODUCTION

The presence of voids under pavements or behind tunnel linings is very likely to result in settlement or structural collapse. However, a characteristic of such voids is that they cannot be detected easily by visual inspection. To effectively locate voids using non-destructive methods is not easy, but one method using radar has been proposed. The advantage of radar is that it can be used to survey a broad area at relatively high speed. Consequently, radar can be regarded as the optimum method for detecting voids under the pavements or behind tunnel linings.

More than simply judging the existence of voids under pavements or behind tunnel linings, this research aims to develop a non-destructive test (NDT) capable of quantitative analysis and evaluation of voids. In order to achieve these goals, the following issues are investigated in this research: (i) an identification system for the size (shape) and location of voids from image data; (ii) the prediction of void thickness by low-resolution radar; (iii) an estimation method on for void volume using three-dipole radar (based on the previous results). The results of this work verify the possibility of a labor-saving NDT system using radar. Subsequently, experiments are conducted to detect the volume of voids under non-reinforced concrete pavements (or tunnel linings) quantitatively.

## 2. ANALYSIS METHOD

### 2.1 Reconstitution of Void Shape

It is known that output signal of radar propagates with a certain beam width. A radar image reflected from an object is broader than the original shape and size of the object. This is because, when a radar pulse is incident at an oblique or normal angle, the reflected radar pulse depends on the geometric configuration of the radar transmitter and the object.

As shown in Figure 1, if the distance between the transmitter and the receiver is small compared to the depth of the object, the radar image from a void with a circular cross section is reconstituted from a reflected radar pulse because a propagation time of an oblique direction (thick line) is plotted in vertical direction (dotted line) as a response time (depth). Accordingly, the reflected radar image of a void with circular cross section becomes broader, as shown in Figure 2. At this time, if the direction of maximum amplitude change of radar return indicates the direction of reflected radar pulse from a certain point of void surface, the original shape of the void can be traced from the radar image by the relationship between the gradient vector of the image and the circular transform of the vertical direction signal. This new algorithm for the shape reconstitution of voids can be explained as follows:

First, as shown in figure 2, a circle is drawn with a radius of depth  $y_n$  for each  $x$  in the range from  $n=0$  to  $m$ , where the center coordinate is  $(x_n, 0)$ . This can be expressed by equation (1). Next, we calculate the gradient vector  $G(x_n, y_n)$  at coordinate  $(x_n, y_n)$  using equation (2) and the slope of the normal vector using equation (3). In this case, a straight line parallel to the normal vector and passing through coordinate  $(x_n, 0)$  can be drawn according to equation (4).

$$\sum_{n=0}^m (x - x_n)^2 + y^2 = y_n^2 \quad (1)$$

$$G(x_n, y_n) = \frac{\partial I(x_n, y_n)}{\partial x} / \frac{\partial I(x_n, y_n)}{\partial y} \quad (2)$$

where  $I(x_n, y_n)$  is the amplitude of the radar return

$$\tan \theta_n = \frac{1}{G(x_n, y_n)} \quad (3)$$

$$\sum_{n=0}^m y = \tan \theta_n (x - x_n) \quad (4)$$

$$y_n = c_s c_r y_{n0} \quad (5)$$

where  $c_r$  is a correction factor for the refraction of electromagnetic waves,  $c_s$  is a correction factor for specified properties of the antenna, and  $y_{n0}$  is  $y_n$  before correction.

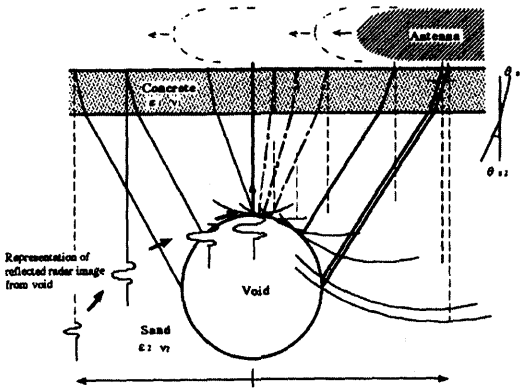


Figure 1. Representation of reflected radar image of void

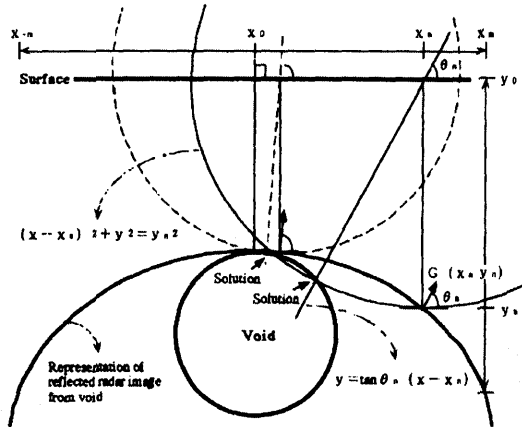


Figure 2. Concept behind shape reconstitution of void

Consequently, the original shape of the void can be restored by connecting the intersections between the circles of equation (1) and the straight lines of equation (4). At this time, it is better to calculate for data over a threshold value of intensity (amplitude). However, the refraction of electromagnetic waves has to be taken into account as the relative dielectric constant of the medium changes because the sub-surface material usually has complicated boundary conditions or non-homogeneities.

This method is, however, difficult to apply to special cases when the frequency domain of the radar is unsuitable for inspection purposes or the condition of the sub-surface material itself is too heterogeneous. As a result, it is necessary to introduce and determine certain correction factors in advance if the original horizontal resolution of the object is to be restored. In general, the correction factor for specified properties of the radar can be determined by adjusting the horizontal resolution (in relation to a fixed direction or beam width) to real the horizontal length of test objects. Using equation (5), correction factors can be calculated not only for specified properties of the radar but also for refraction. If these correction factors, the shape reconstitution of voids can be expected to improve.

## 2.2 Estimation of Void Thickness

A void under a concrete slab (such as a pavement or tunnel lining) will cause radar returns (reflected radar pulses) to appear as shown in Figure 3. Since the dielectric constant of concrete or soil is greater than that of air, the reflection coefficient at a concrete/void or soil/void interface is positive. However, the reflection coefficient at a void/soil interface is negative. Thus, the reflected pulses from these two boundaries are of different polarities, as indicated in Figure 3.

The time separation between the pulses from the top and bottom of the void is proportional to the void thickness in the direction of incidence. The relationship between an air void thickness,  $D(\text{cm})$ , and pulse separation  $t(\text{nanoseconds})$  is as follows<sup>1)</sup>:

$$t = \frac{2D}{v} = \frac{2D\sqrt{\epsilon_r}}{c} = \frac{D\sqrt{\epsilon_r}}{15} \quad (6)$$

where  $\epsilon_r$  is the relative dielectric constant of the medium and  $c$  is the speed of light ( $3 \times 10^8 \text{m/s}$ ).

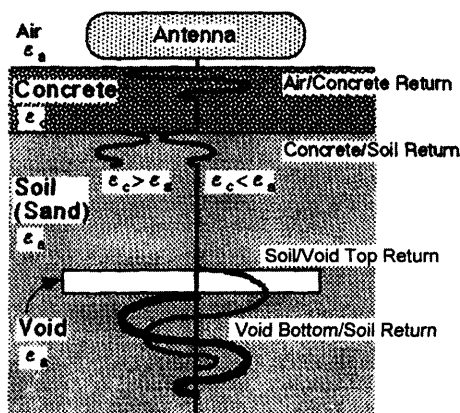


Figure 3. Behavior of radar returns at multiple boundaries.

The radar used in this study (central frequency: 600MHz) has a pulse length of about 1.7 nanoseconds. Thus, a void thickness must be greater than 26cm if the reflected radar pulses from the concrete or soil/void and void/soil interfaces are not to overlap in time. Since many voids are expected to be less than 26cm, the radar returns from the top and bottom of the void will overlap. However, the amplitude of the composite pulse will vary depending on the time separation between the two pulses. Thus the amplitude characteristics of the radar return can be used to estimate void thickness even if actual radar returns from the top and bottom of the void cannot be distinguished.

The regression relationship between void thickness and the amplitude characteristics of the radar return is considered in this study. For the purpose of examining this regression relationship, the following experiments were carried out. The experimental design is indicated in Table 1.

First, the regression relationship between the maximum amplitude characteristics of the radar return and void depth was examined under conditions of constant thickness and surface area. Next, to be examined was the regression relationship between the maximum amplitude characteristics of radar return and the void surface area under conditions of constant thickness and depth. Last, the regression relationship between maximum amplitude and void thickness was examined under conditions of constant depth and surface area. The equation given below was obtained by arranging the regression equations as above using a proportional expansion of each equation.

In particular, equation (7) includes the parameters STC. STC is a function compensating for the exponential attenuation of electromagnetic waves according to additive propagation distance (depth) in a dielectric medium. This function is useful in that it allows detection of the radar return from objects at comparatively deep locations. However, it has different properties depending on the actual radar apparatus used. Equation(7) allows STC to be applied to any radar apparatus.

$$T_{STC_x}(cm) = \left[ \frac{4020 - R_{m/STC1} \frac{A}{1.6 \times 10^6 B} e^{-0.0378D(cm)}}{49.1} \right] \quad (7)$$

where,  $T_{STC_x}$  is the estimated value of void thickness and  $R_{m/STC_x}$  is the maximum amplitude of the radar return from the void when parameter STC is not applied. Coefficients A and B can be calculated by equation (8), which is obtained from the relationship between maximum amplitude of the radar return and the void depth when STC is applied. D is the void depth.

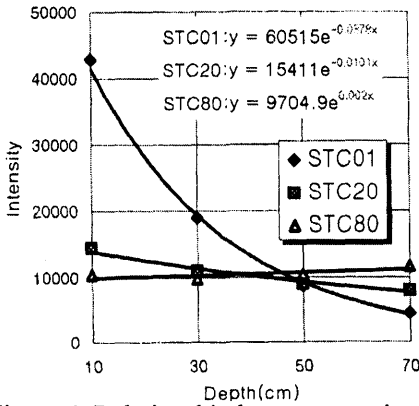


Figure 4. Relationship between maximum amplitude characteristics of radar return and void depth when STC 1, 20, and 80 are applied

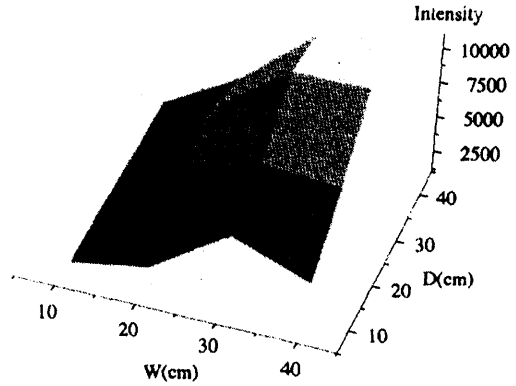


Figure 5. Relationship between maximum amplitude characteristics of radar return and void surface area

$$R_{m/STC_x} = Ae^{-BD(cm)} \quad (8)$$

where,  $R_{m/STC_x}$  is the maximum amplitude of the radar return from the void when STC is applied.

Table 1. Experimental design for estimation of void thickness (W, D, and H are defined in Figure 11)

	Void condition ( Unit: cm )	
	Fixed factor	Variable factor
Change in void depth	W40,D40,H10	Depth 10,30,50,70
Change in void surface area	Depth30,H10	
	W10	D10,20,30,40
	W40	D10,20,30,40
	D10	W20,30,40
	D40	W20,30,50
	W20	D20
	W30	D30
	W50	D50
Change in void thickness [H]	Depth30, W40,D40	H2,10,20,30

The values of STC used this study range from 1 to 80. The larger this number becomes, the greater the attenuation compensation. The relationship between the maximum amplitude of the radar return and void depth is compared in Figure 4 for representative STC values of 1, 20, and 80. As is clear from this figure, the maximum amplitude of radar return varies not only with void depth but also with STC. Thus, a suitable STC has to be chosen according to the properties of the radar apparatus in use when this function is applied.

This method is valid only for the estimation of void thickness when the void surface area is greater than  $W40\text{cm} \times D40\text{cm}$ . [Definitions of W and D are given in Figure 11.] The reason for this is that the maximum amplitude of the radar return from voids of this surface area is uniform, as shown in Figure 5. Thus, void thickness can be estimated from equation (7) regardless of the influence of void surface area only if the void surface area is greater than  $W40\text{cm} \times D40\text{cm}$ .

### 2.3 Estimation of Void Volume

To acquire directional information and estimate the volume of three-dimensional voids, three-dipole radar was used. As shown in figure 6, four microwave polarization modes can be obtained with different arrangements of the antennas. The dispersion matrix for these microwave polarization modes can be defined as follows:

$$[S] = \begin{bmatrix} S_{xx} & S_{xy} \\ S_{yx} & S_{yy} \end{bmatrix} \quad (9)$$

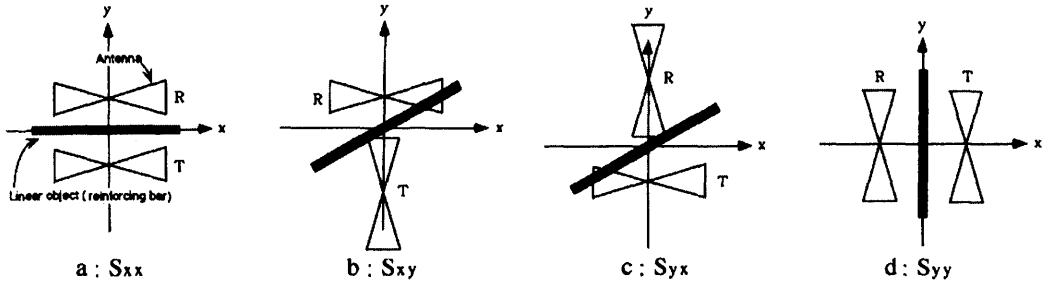


Figure 6. Microwave polarization modes

Ultimately, the following equation (10) for each element of the dispersion matrix can be obtained for a three-dipole antenna, as shown in Figure 7.

$$\begin{aligned} S_{xx} &= -\langle E_1^R | E_2^T \rangle - \langle E_3^R | E_1^T \rangle \\ S_{xy} &= \frac{1}{\sqrt{3}} \left( \langle E_1^R | E_2^T \rangle - \langle E_3^R | E_1^T \rangle \right) \\ S_{yy} &= -\frac{1}{3} \langle E_1^R | E_2^T \rangle - \frac{1}{3} \langle E_3^R | E_1^T \rangle - \frac{4}{3} \langle E_2^R | E_3^T \rangle \end{aligned} \quad (10)$$

where  $E_n^m$  is the vector of electrical field radiation from the antenna, with m indicating transmission T or receiving R and n indicating the element number of the antenna.

Therefore, the following equation (11) can be defined as the dispersion matrix [S]'in a new X,Y coordinate system rotated by angle  $\phi$  from the x, y coordinate system, as shown in Figure 8.

$$[S]' = |\phi| |S| |\phi|^T \quad \text{where, } |\phi| = \begin{vmatrix} \cos \phi & \sin \phi \\ -\sin \phi & \cos \phi \end{vmatrix} \quad (11)$$

This process elucidates the following.

In the case of parallel microwave polarization modes ( $S_{xx}$ ,  $S_{yy}$ ), the reflected radar pulse has a maximum amplitude when a linear object is oriented at an angle ( $\phi$ ) of 0 or 90 degrees. Furthermore, the detection range of object shape in this mode is broader than in the other modes. However, in the case of the perpendicular microwave polarization modes ( $S_{xy}=S_{yx}$ ), the reflected radar pulse has a maximum amplitude when the linear object is oriented at 45 degrees.

Consequently, the shape or orientation of voids can be found approximately from the calculated dispersion matrix of each microwave polarization mode ( $S_{xx}$ ,  $S_{yy}$  and  $S_{xy}=S_{yx}$ ) after a radar investigation. Also, the shape discrimination factor R, as expressed by equation (12), is defined as the ratio of the dispersion matrix on the Y-axis to that in the X-axis in a new rectangular coordinate system XY when a parallel microwave polarization mode ( $S_{xx}$ ,  $S_{yy}$ ) is applied. The conception of the shape discrimination factor according to object shapes is as shown in Figure 9 in the case where the X-axis is taken to be in the longitudinal direction. Three types of object shape, that is, linear, co-axial, and non-linear non-co-axial are defined in this study. The linear shape expresses objects which are predominantly one-dimensional, such as pipes or reinforcing bars. Co-axial expresses objects which have similar dimensions in the two axes of the XY coordinate system. Non-linear and non-co-axial shapes are all objects which fall outside these two definitions.

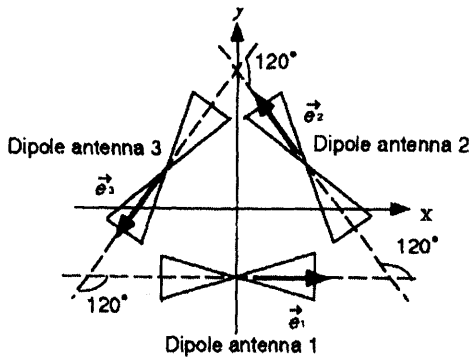


Figure 7. Scheme of three-dipole antenna elements

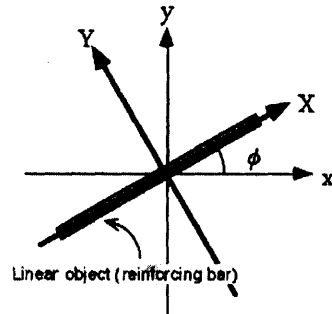


Figure 8. Transformation to new coordinate system

Using the methods described above, the thickness and surface shape of a void can be determined. Finally, the void volume can be estimated using the algorithm described below. Noting that this algorithm applies only when the surface shape of the void is co-axial.

Figures 10 and 11 illustrate how void volume is estimated using three-dipole radar. The parallel microwave polarization mode at each angle to the central coordinate system of the objects can be obtained from an angular transformation of the central coordinate system using equation (19). Consequently, the parallel microwave polarization mode over an angle from 0 degrees to 360 degrees can be calculated from a one-directional radar investigation when the surface coverage of the antenna is sufficiently broader than the void surface area.

Consequently, the void volume can be calculated by summing the cross sectional areas at each angle from 0 degrees to 360 degrees, as shown in Figure 10. The cross-sectional area at each angle can be calculated from the results of the reconstitution of void shape and the estimation of void thickness described above. The resulting computation process for void surface area and void volume are expressed respectively by equations (13) and (14).

	$S_{xx}, S_{yy}$ No response  $S_{xy}, S_{yx}$ Good response (Maximum at $\phi = 45^\circ$ )	$R = 0$ : Linear
	Examples : reinforcing bars, pipes, cables	
	$S_{xx}, S_{yy}$ No response  $S_{xy}, S_{yx}$ Good response (Maximum at $\phi = 45^\circ$ )	$0 < R < 1$ : Non-linear & non-co-axial
	Examples : ovals, rectangles	
	$S_{xx}, S_{yy}$ Good response  $S_{xy}, S_{yx}$ No response	$R = 1$ : Co-axial
	Examples : circles, squares	

$$R = \frac{S_{yy}}{S_{xx}} \quad (12)$$

$$A_1 = \frac{1}{2} a_1 a_0 \sin \theta_d \quad (13)$$

$$V_1 = \frac{1}{2} a_1 a_0 \sin \theta_d t_1$$

$$V_2 = \frac{1}{2} a_2 a_1 \sin \theta_d t_2$$

$$V_3 = \frac{1}{2} a_3 a_2 \sin \theta_d t_3$$

⋮

$$V_n = \frac{1}{2} a_n a_{n-1} \sin \theta_d t_n \quad (14)$$

Figure 9. Shape discrimination factors for objects (voids) by transformation of microwave polarization mode

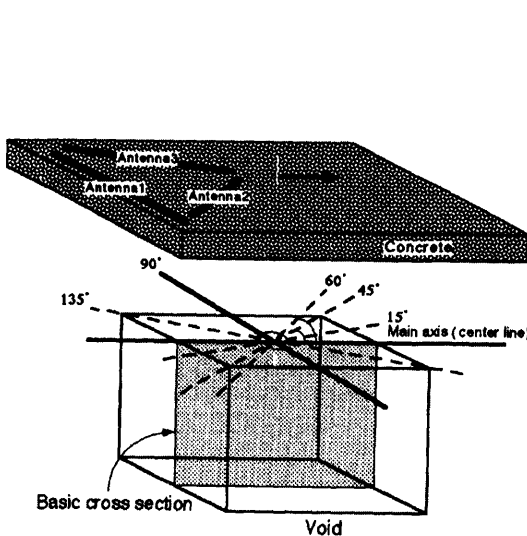


Figure 10. Estimation of void volume

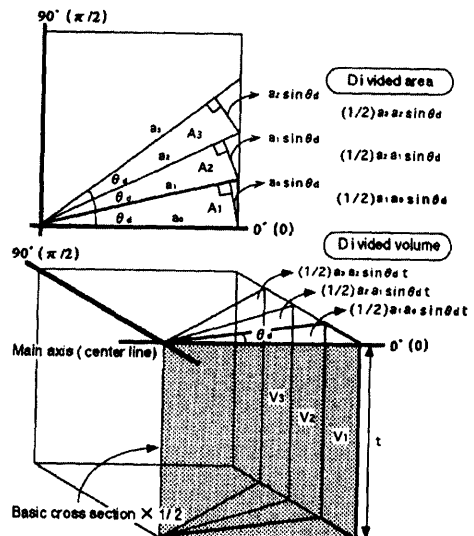


Figure 11. Calculation process for void surface area (upper) and void volume (lower)

### 3. EXPERIMENTAL

#### 3.1 Experimental conditions

Experiments on the detection of voids under pavements and behind tunnel linings were performed under two experimental conditions. As one example, Figure 12 shows the experimental conditions in the case of voids with a square plane form (co-axial type) and various thicknesses (10cm, 20cm) under a non-reinforced concrete slab. The other case is shown in Figures 13 and 14, where voids of circular plane form (co-axial type) and rectangular form (non-linear non-co-axial type) are under a polyurethane sheet.

Mix conditions of the concrete slab were w/c: 55%; s/a; 46%, slump; 5cm, maximum aggregate size: 22mm; and compressive strength at 28days; 240kg/cm<sup>2</sup>. In all cases, the water content of the sand in the material under the concrete slab (or polyurethane sheet) was from 1.7 to 3.4%.

#### 3.2 Measurement system

Ground probing radar was used for measurements in this experiment. The frequency of this radar is from 20 MHz to 1GHz (central frequency: 600MHz) and the antenna system is a 3-dipole type.

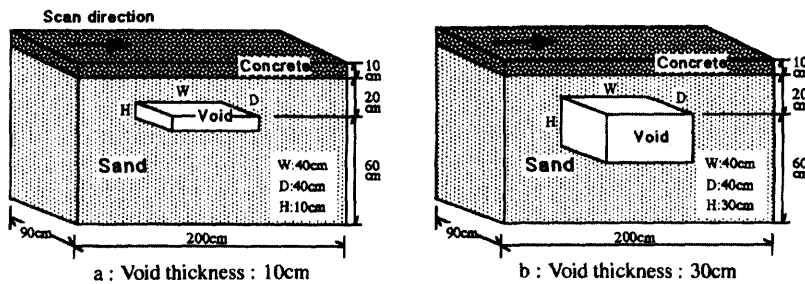


Figure 12. Experimental conditions for detecting voids of square plane form (co-axial type) and of different thicknesses (10cm, 30cm) under non-reinforced concrete slab

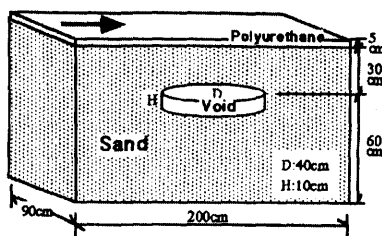


Figure 13. Experimental conditions for detecting voids of circular plane form (co-axial type) under polyurethane sheet

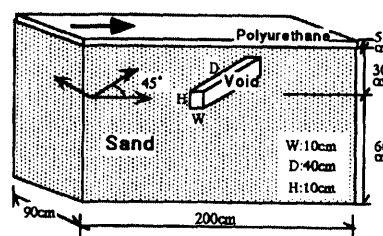


Figure 14. Experimental conditions for detecting voids of rectangular form (non-linear and non-co-axial type) under polyurethane sheet

### 4. RESULTS AND DISCUSSION

Figure 15 shows the radar image (B scan) resulting from scanning the radar across the void under the experimental conditions given in Figure 12a. The reconstituted void shape according to the proposed method is shown in Figure 16. This is analyzed result agrees well with the actual experimental arrangement in Figure 12a, and the target void is easily

distinguished without noise.

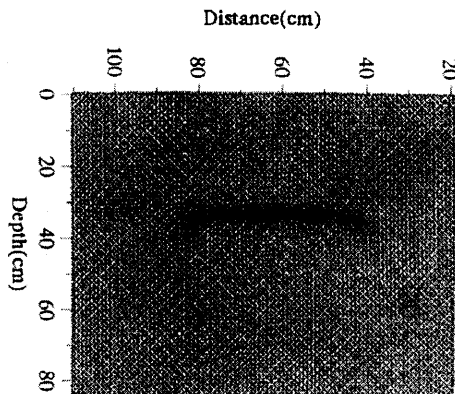
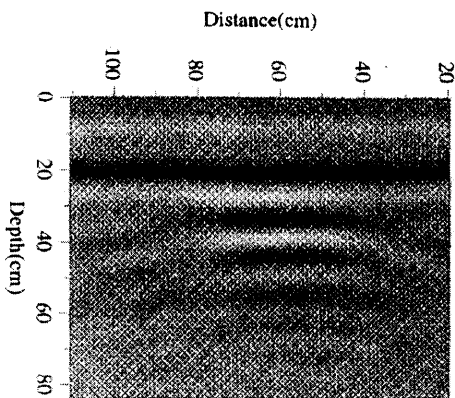


Figure 15. Radar image ( $S_{yy}$ ) of Figure 12a      Figure 16. Processed image (shape reconstruction) from Figure 15

Furthermore, the radar images shown in Figures 17 ~ 20 are the calculation results of the dispersion matrix of microwave polarization mode for the various void conditions in Figures 12a, 13, and 14. This dispersion matrix was calculated using equations (10) and (11). Of these results, Figures 15 and 17 show images of the parallel microwave polarization mode  $S_{yy}$ , while the perpendicular microwave polarization mode  $S_{xy}=S_{yx}$  is given in figure 12a. Further, Figure 18 shows parts of the dispersion matrix of the parallel microwave polarization mode over an angle from 0 degrees to 360 degrees as obtained from an angular transformation of the central coordinate system using equation (10). Figures 19 and 20 show radar images of the dispersion matrix of  $S_{yy}$  and  $S_{xy}=S_{yx}$  for Figure 14, respectively. From these results, the following understanding is obtained.

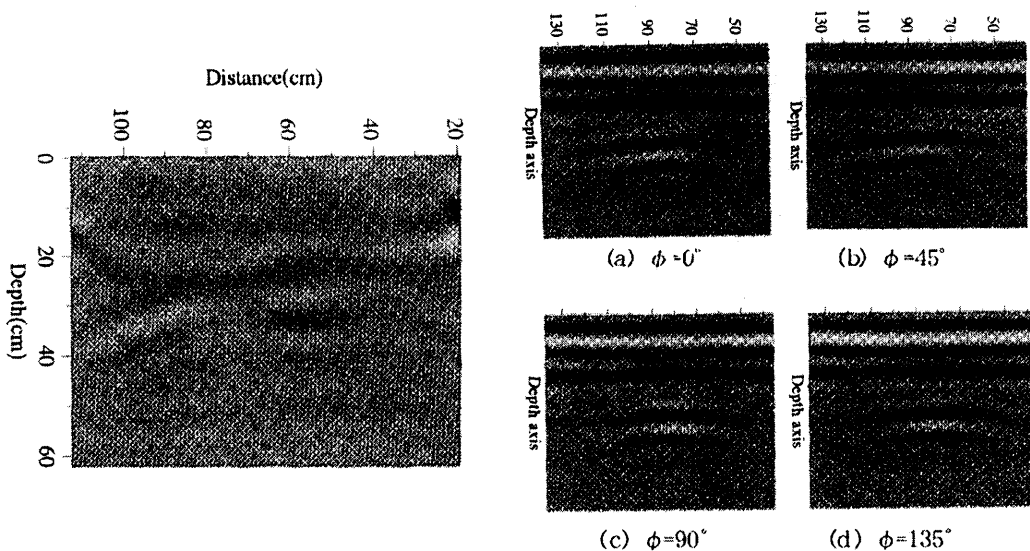


Figure 17. Radar image ( $S_{xy}=S_{yx}$ ) of figure 12a      Figure 18. Radar image ( $S_{yy}$ ) of figure 13 in new coordinate system (in case of  $\phi = 0^\circ, 45^\circ, 90^\circ, \text{ and } 135^\circ$ )

In the case of Figure 19 (the radar image ( $S_{yy}$ ) of Figure 14), it is clear that non-linear and non-co-axial voids cannot be detected easily because the amplitude of the radar return is very weak in the parallel microwave polarization mode  $S_{yy}$ . But the amplitude of the radar return peaks in the perpendicular microwave polarization mode  $S_{xy}=S_{yx}$ . Thus, it can be assumed that the void shape in Figure 14 is non-linear and non-co-axial ( $0 < R < 1$ ) and is oriented at an angle ( $\phi$ ) of 45, according to the definition of shape discrimination factor of the objects (voids) as shown in Figure 9.

In the case of Figure 15 (the radar image ( $S_{yy}$ ) of Figure 12a), it can be assumed that the void shape is co-axial because the amplitude of the radar return in the parallel microwave polarization mode  $S_{yy}$  (Figure 15) is greater than in the perpendicular microwave polarization mode  $S_{xy}=S_{yx}$  (Figure 17).

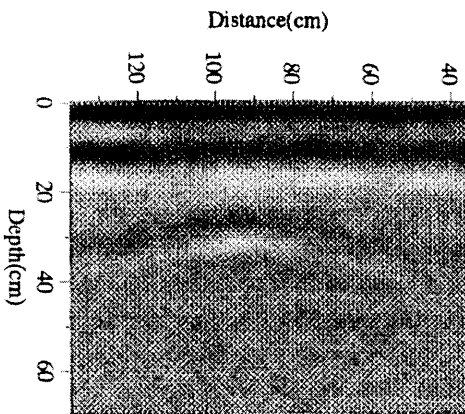


Figure 19. Radar image ( $S_{yy}$ ) of Figure 14

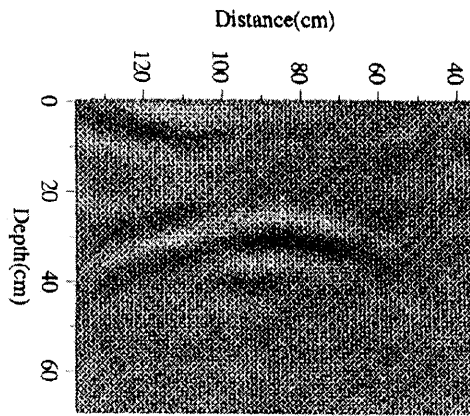


Figure 20. Radar image ( $S_{xy}=S_{yx}$ ) of Figure 14

	<p>Co-axial void (Square plane form)</p> <p>Estimated volume : 80%</p>
	<p>Co-axial void (Circular plane form)</p> <p>Estimated volume : 95~105%</p>
	<p>Non-linear &amp; non-coaxial void</p> <p>Estimated volume : -</p>

Figure 21. Results of co-axial void volume

Also, in the case of Figure 18 (the radar image ( $S_{yy}$ ) of figure 13), it can be assumed that the void is of perfect co-axial form like a circle because the radar image at all angles from 0 degrees to 360 degrees has the same pattern and amplitude.

The estimated volumes of co-axial voids by this method are shown in Figure 21. The accuracy of estimated volume for these co-axial voids is as high as 80% in the case of a square plane form and 95 ~ 105 % in circular plane form. However, it is not possible to estimate the volume of non-co-axial voids. On the other hand, it was clarified that the response varies with changing void geometry and thus there is a possibility of identifying the geometry and orientation of specific voids by this method.

## **5. CONCLUSIONS**

1. The availability of a new method for detecting the shape and estimating the volume of voids in or under non-reinforced concrete has been verified. The precision of the results obtained by this proposed method is considered acceptable after an analytical and experimental investigation.
2. In the case of estimating void volume, it should be noted that the new method is only available for co-axial shape voids, such as voids with a square plane form or circular plane form, if three-dipole ground-probing radar is used. However, it has also been clarified that the response of microwave polarization modes varies with changes in void geometry and thus there is a possibility of identifying the geometry and orientation of specific voids by the proposed method.

## **Acknowledgements**

This study was carried out at the University of Tokyo, Department of Civil Engineering, as a part of the author's doctoral programme. The first authors would like to thank Mr. D. Sakamoto of Fujita Corporation for his kind contribution in performing the experiments.

## **References**

- [1] J.R.Moore, J.D.Echard and C.G.Neill, "Radar Detection of Voids under Concrete Highways", IEEE International Radar Conference, pp.131~135, 1980
- [2] K. Murasawa, H.Nishizaki, C.Jyomuta, N.Kimura and H.Obara, "Subsurface Radar with Three Antenna Elements Based on Scattering Theory", Michuizousengibo, Japan, No.152, 1994.6
- [3] A.D.Olver et al., "Portable FM-CW Radar for Locating Buried Pipes", Proc. International Conference Radar-82, pp.413-418, 1982
- [4] K.Ueno, N.Osumi, "Underground Pipe Detection based on Microwave polarization Effect", Proc. ISNCR, pp.673-678, 1984
- [5] S.K.Park, T.Uomoto, "Radar image Processing for Detection of Shape of Voids and Location of Reinforcing Bars on or under reinforced concrete", International Conference Non-Destructive Testing in Civil Engineering (NDT-CE '97) Proc.Vol.1 and 2, Liverpool, UK, 1997. 4
- [6] S.K.Park, T.Uomoto and M. Yoshizawa, "Nondestructive Test for Concrete Structures Using Radar (3)", Journal of Institute of Industrial Science, University of Tokyo, Vol.48, No.5, 1996
- [7] S.K.Park, T.Uomoto and M. Yoshizawa, "Quantitative Evaluation of Voids under Concrete Pavement Using Radar", Proceedings of the Japan Concrete Institute, Vol.18, No.1, 1996